**EUROPEAN ORGANIZATION FOR NUCLEAR RESEARCH**

**Letter of Intent to the ISOLDE and Neutron Time-of-Flight Committee**

# Shape transition at $N = 60$: Development of neutron-rich Sr beams

September 28, 2021

K. Wimmer[1], S. Bhattacharjee[2], P. Bender[3], E. Clement[4], K. Chrysalidis[5], S. Freeman[6], L. Gaffney[7], J. Gerl[1], M. Górska[1], T. Hüyük[8], W. Korten[9], S. Rothe[5], D. Sharp[6], S. Stegemann[5], M. Zielińska[9]

[1]*GSI (Germany),* [2]*Czech Technical University (Czech Republic),* [3]*U Mass Lowell (USA),* [4]*GANIL (France),* [5]*CERN-ISOLDE (Switzerland),* [6]*U Manchester (UK),* [7]*U Liverpool (UK),* [8]*CSIC (Spain),* [9]*CEA Saclay (France)*

**Spokesperson:** Kathrin Wimmer, k.wimmer@gsi.de
**Contact person:** Sebastian Rothe, sebastian.rothe@cern.ch

**Abstract:** We propose to investigate the $N = 60$ spherical-deformed shape transition in neutron-rich strontium isotopes by two types of experiments. Multi-step Coulomb excitation of odd-$A$ isotopes $^{95,97}$Sr will provide the missing data on the deformation of these two isotopes approaching the transition and further clarify the role of shape coexistence for $N < 60$. With two-neutron transfer reactions we plan to specifically probe the $0^+$ states in $^{96,98}$Sr and their mixing.

With this letter of intent, we plan to measure the yields of neutron-rich Sr beams and study two possible production schemes, laser ionization or extraction as a molecular beam from the target. For the proposed physics experiments, we are especially interested in rates for $^{94-98}$Sr beams at the HIE-ISOLDE Miniball and ISS beam-lines.

**Requested shifts:** 3 shifts for yield measurements and tests, 2 shifts stable beam tuning

# 1    Motivation

Nuclei around $N = 60$ show one of the most dramatic shape transitions in the nuclear chart. Between $^{90}$Zr, with a magic number for the neutrons, $N = 50$, and the sub-shell closure at $N = 56$, the Zr nuclei are spherical or only weakly deformed in their ground states. In $^{100}$Zr, at $N = 60$, the ground state is suddenly strongly deformed. This is evidenced by a rise in the two-neutron separation energy [1] and a strong increase in the charge radius [2]. Fig. 1 shows the deformation parameter $\beta_2$ of nuclei in this region. The values, extracted from laser spectroscopy
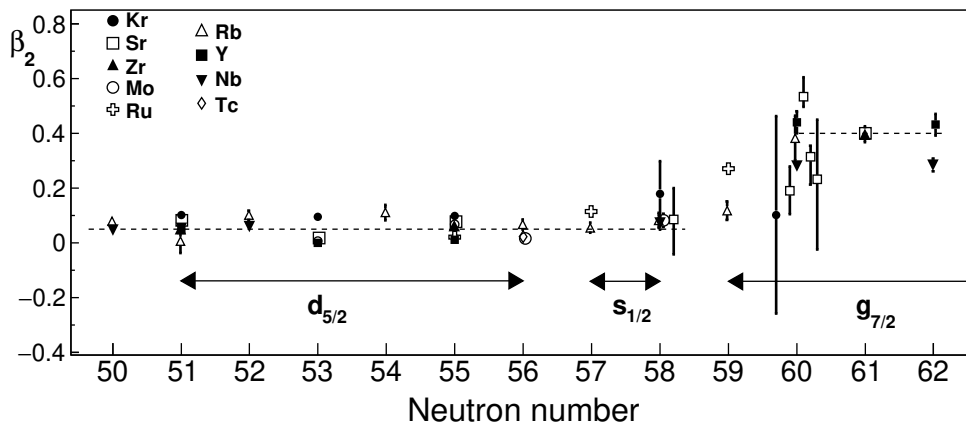


Figure 1: Deformation parameters $\beta_2$ of $A \sim 100$ nuclei. Values are extracted from spectroscopic quadrupole moments obtained in laser spectroscopy experiments or from Coulomb excitation of $2_1^+$ states of even-even isotopes. Figure from [3].

and Coulomb excitation experiments, show a marked step at $N = 60$ from $\beta_2 \approx 0.05$ to values around 0.4. The occurrence of deformation is explained by the strong proton-neutron correlations originating from the large overlap of the proton $0g_{9/2}$ and neutron $0g_{7/2}$ orbitals, which are filled in this region [4]. Increased occupation of the $\nu 0g_{7/2}$ orbital leads to the promotion of protons from the $1p_{1/2}$ to the $0g_{9/2}$ orbital, i.e. across the $Z = 40$ sub-shell closure. Similarly, the increased occupation of the $\pi 0g_{9/2}$ orbital can increase the neutron occupation of the $\nu 0g_{7/2}$ orbital. The mutual interaction of protons and neutrons thus leads to collective effects in nuclei at and beyond $N = 60$. In addition, the nuclei around $N = 60$ are a prime example of shape coexistence with low-lying $0^+$ states and strong electric monopole transitions $\rho^2(E0)$ between them [5]. Before $N = 60$, the ground state is spherical, while excited $0^+$ states are interpreted as deformed intruder states. At $N = 60$, an inversion happens, the ground state is now strongly deformed, with a large $B(E2)$ value to the low-lying $2_1^+$ state and an excited spherical $0_2^+$ state. Recently, the Zr nuclei were calculated using the Monte-Carlo shell model (MCSM) approach [6]. The inversion of shapes and configurations is attributed to strong central and tensor components of the proton-neutron interaction lowering the $\nu g_{7/2}$ and $h_{11/2}$ orbitals as the proton $0g_{9/2}$ occupation increases following the earlier interpretation of Ref. [4]. Then, the neutron occupation of the deformation driving orbitals increases, leading to a polarization of the proton wave function. This coherent behavior of protons and neutrons is self-reinforcing, causing very strongly deformed ground states in $^{100}$Zr and for neutron numbers beyond.
Regarding the Sr isotopes, the ground states are spherical up to $^{94}$Sr [7, 8]. $^{96}$Sr, with $Z = 38$ and $N = 58$, lies just at the $N = 60$ shape transition, where a rapid change in the ground state deformation has been observed [9–11]. The ground state of $^{96}$Sr is still only very weakly deformed, however, a detailed investigation of the structure of the $0^+$ states by a $(d, p)$ transfer

reaction [12] showed that the configuration is not of simple $(2s_{1/2})^2$ nature[1]. The shape transition in the Sr isotopes happens thus between $^{95}$Sr and $^{98}$Sr. We therefore propose to probe this transition region by additional experiments.

While Sr beams have been produced at ISOLDE before in experiment IS451 [9], the values are not included in the yield database. In the previous experiments, neutron-rich Sr nuclei have been produced by different methods, and laser ionization is an additional option, which up to now has only been done at TRIUMF. Following the recommendation of the target group, we therefore propose to measure the yields of neutron-rich Sr nuclei and explore the production methods.

# 2 Proposed future experiments

After successful yield measurements, we would like to study the shape transition at $N = 60$ by two types of experiments. To complement the data shown in Fig. 1, we plan to study low-energy, multi-step Coulomb excitation of the odd-$A$ isotopes $^{95}$Sr and $^{97}$Sr. Both have $J^\pi = 1/2^+$ ground states, which prevents the determination of deformation properties by laser spectroscopy. Coulomb excitation will shed more light on the band structure and the deformation in these two isotopes. The study of two-neutron transfer reactions with even Sr beams will provide a sensitive probe of the wave function composition of the final states in $^{96,98}$Sr. This will shed new light on the nature of the $0^+$ states.
Here, we provide some details of the goals for the individual isotopes.

## 2.1 $^{95}$Sr

MCSM calculations [6, 13] predict the coexistence of an oblate ground state band, prolate excited intruder states, and a triaxial deformed band built on the low-lying $7/2^+$ state, as shown in Fig. 2. It should be noted, that the calculations predict a much larger level density for $^{95}$Sr than experimentally observed and generally the collectivity in low-lying states of this nucleus is over-predicted. On the other hand, shell model calculation in a limited space presented in Ref. [14] are in good agreement with the experimental results for the excitation energies and spectroscopic factors, however, predict smaller $B(E2)$ values. A Coulomb excitation experiment would yield $B(E2)$ values and quadrupole moments which directly probe the collectivity.

## 2.2 $^{97}$Sr

The MCSM calculations shown in Fig. 2 [6, 13] predict two bands in $^{97}$Sr. In contrast to the experimental results, where a $1/2^+$ ground state is firmly established [11], the calculations predict a $3/2^+$ ground state which is the band head of a prolate deformed $3/2^+$, $7/2^+$, $5/2^+$ sequence. The $B(E2)$ values between states of similar structure are very large. Calculations based on the Interacting Boson Fermion Model are presented in Ref. [15] and these give a better description of the level scheme than the MCSM calculations, but discrepancies with the $B(E2)$ and $B(M1)$ values extracted from measured lifetimes are seen. Unfortunately, due to some spin-parity ambiguities, detailed comparisons cannot be made yet. Weak population of $^{97}$Sr ground state in $(d,p)$ transfer suggests a different structure than the ground state of $^{96}$Sr [14]. The

---

[1]Owing to the almost pure $\nu 2s_{1/2}$ ground state configuration of the $1/2^+$ ground state in $^{95}$Sr, the $(d,p)$ transfer is mostly sensitive to the neutron $(2s_{1/2})^2$ configuration in the final $0^+$ state.
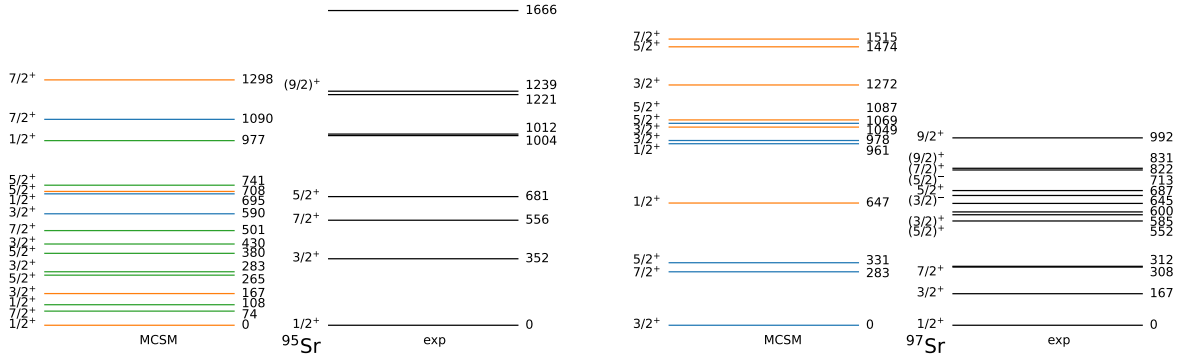
Figure 2: Calculated levels compared to (selected) experimentally known states. Levels are labeled with their energy and, where known, spin and parity. For the MCSM calculations prolate (oblate) states are marked in blue (orange). States with calculated triaxial deformation are shown in green. Note that for $^{97}$Sr the triaxial degree of deformation could not yet be assessed in the calculations due to computational limitations.

latter is suggested to be weakly oblate deformed [9], which could indicate a deformed ground state already at $N = 59$. $^{97}$Sr was also studied at ILL, where the internal decay of the $(9/2^+)$ isomeric state was investigated and the lifetimes of several states could be measured using the fast-timing technique [15]. Based in the comparison to the IBFM calculations $5/2^+$ is favored, but the population in the transfer reaction suggests a $3/2^+$ assignment[2]. It is of special interest to identify experimentally the band structures in $^{97}$Sr and clarify their deformation.

## 2.3 $^{96}$Sr

The low-energy excited $0^+_{2,3}$ states in $^{96}$Sr are among the most prominent examples of shape coexistence across the nuclear landscape. The electric monopole transitions strength between the two excited $0^+$ states, $\rho^2(E0) = 185 \cdot 10^{-3}$ [16], is the largest known in the nuclear chart [5]. The systematics of $0^+$ states is shown in Fig. 3. MCSM calculations for the Sr isotopes [6, 10]
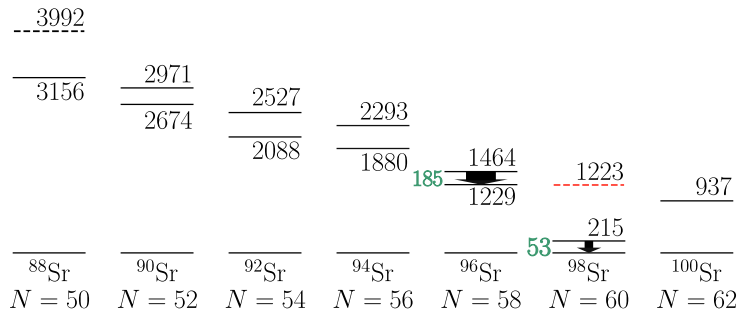


Figure 3: Systematics of $0^+$ states in even-even Sr isotopes. Excitation energies are in keV. Two excited $0^+$ states in $^{94}$Sr were discovered recently and complete the systematics [17]. Also shown are the electric monopole transitions with strength $\rho^2(E2) \cdot 10^3$ [16, 18] in green.

---

[2]A $5/2^+$ assignment would imply a significant vacancy in the $1d_{5/2}$ orbital in the ground state of $^{96}$Sr.

4

describe well the level schemes and $B(E2)$ values of $^{94}$Sr and $^{98}$Sr but predict already substantial deformation for $^{96}$Sr. For all these theoretical calculations the agreement with the experimental information is much better in $^{98}$Sr and $^{98}$Zr than for $^{96}$Sr. It is therefore required to probe in addition the details of the wave function through spectroscopic factors and two-nucleon amplitudes from the $^{94}$Sr$(t,p)^{96}$Sr reaction. We previously studied $^{96}$Sr in a $(d,p)$ transfer reaction experiment at TRIUMF [12, 14]. Most notably, we have determined the spectroscopic factors for the $d(^{95}$Sr$,p)$ reaction to the first three $0^+$ states in $^{96}$Sr. Our results show a surprisingly strong population of an excited spherical configuration in $^{96}$Sr, which itself is strongly mixed with a deformed ($\beta = 0.31(3)$) configuration, giving rise to two $0^+$ states at 1229 and 1465 keV. This suggests the occurrence of three distinct shapes in $^{96}$Sr [12]. With a $(t,p)$ reactions, we will be able to probe other parts of the wave function and get more insights into the structure of the three $0^+$ states.

## 2.4   $^{98}$Sr

The ground state of $^{98}$Sr is strongly deformed. This is evidenced by a large $B(E2; 2_1^+ \to 0_1^+) = 94(3)$ W.u. [19], a $R_{4/2}$ value of 3.0, a regular rotational band that is known up to $J^\pi = 12^+$ from fission studies with large $B(E2)$ values between the band members [20]. Coulomb excitation suggests a strongly prolate deformed ground state and a weakly oblate deformed excited $0_2^+$ state [9, 21]. If the yields are sufficient, the ultimate goal of this study would be the study of the $N = 60$ nucleus $^{98}$Sr by a two-neutron transfer reaction. This would give a measure of the mixing of the spherical and deformed configurations beyond what has been studied in Coulomb excitation [9] and decay experiments [10, 18, 22]. The $(t,p)$ reaction would also probe the tentatively assigned $0_3^+$ at 1223 keV.

# 3   Experimental setup and technique

We propose two types of experiments to investigate the shape transition across $N = 60$. Both use established experimental setups and techniques.

## 3.1   Multi-step Coulomb excitation of odd-$A$ isotopes

For the odd-$A$ Sr isotopes, we propose to study safe Coulomb excitation. In order to obtain good constraints on the transitional and diagonal matrix elements it is proposed to measure on two different targets. For a heavy target, $^{208}$Pb, the safe energy amounts to 4.2 $A$MeV for all scattering angles. For lighter targets, such as $^{120}$Sn or $^{60}$Ni, the safe energy is 3.4 to 3.0 $A$MeV. The experimental setup will consist of the Miniball array and the standard CD detector or the C-REX array, depending on the availability. The choice of target and therefore beam energy will depend on this as well. We estimate that with a beam intensity extrapolated from the earlier REX experiments [21] that about one or two days (3 shifts each) per beam and target combination is sufficient. In order to analyze the Coulomb excitation cross sections, knowledge about the transition multipolarities is also of interest. In $^{95}$Sr, they are known in many cases from a conversion electron measurement following the $\beta$ decay of $^{95}$Rb [23]. Level lifetimes are known in $^{97}$Sr [15] which can be used as a constraint in the analysis and some mixing ratios are also known [24]. Without a reliable estimate of the beam intensity, it is however, difficult to estimate the sensitivity of the proposed measurements to these unknown quantities. Based on the result of the proposed yield test, we are considering an additional $\beta$ decay measurement

for $^{97}$Sr. Fig. 4 shows the results for simulations assuming $5 \cdot 10^4$ particles per second at the Miniball target.
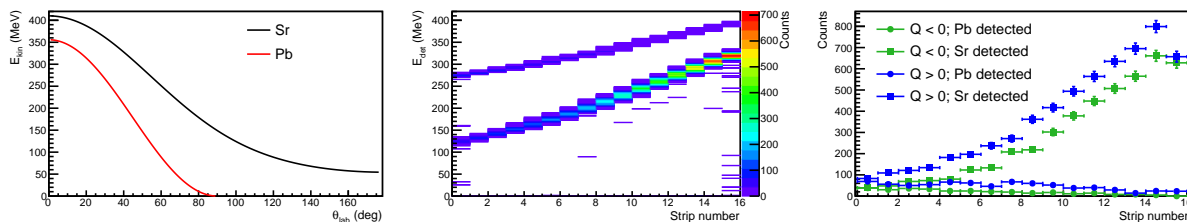


Figure 4: Left: Kinematics of the scattering of $^{97}$Sr on $^{208}$Pb at 4.2 $A$MeV. Middle: Simulation for the number of detected particles in the CD detector as function of the ring number (larger numbers correspond to inner rings, and smaller laboratory scattering angles). Right: Detected $\gamma$-ray yield for $Q > 0$ and $Q < 0$ for the $5/2^+$ state of $^{97}$Sr. The input uses the calculated Coulomb excitation cross sections including $B(E2)$ values and quadrupole moments from the MCSM calculations. Only few states have been included in the cross section calculations.

## 3.2 Two-neutron transfer reactions

We also propose to study the two-neutron transfer reactions with $^{94,96}$Sr beams on a radioactive tritium target. Such a reaction provides information on the underlying wave functions which ultimately govern the properties of these states, that would not be otherwise available. Due to the small energy spacing between the excited $0^+$ states in $^{96}$Sr and $^{98}$Sr (see Fig. 3), the superior energy resolution that can be achieved with the ISOLDE Solenoidal Spectrometer is crucial for this experiment. The missing mass technique is further not suffering from finite lifetimes of the excited states, which in the case of $\gamma$-ray detection reduces the in-beam efficiency significantly [12]. Experiments with a tritium target have been performed in the past at T-REX and Miniball, and the first use of a tritium target at ISS is planned for 2022 (IS696). It is estimated that with a $^{94}$Sr beam intensity of $10^5$ particles per second at the ISS target, the experiment can be performed in about five days (15 shifts). Based on our $(d, p)$ results, we have calculated the DWBA cross sections, including our experimental spectroscopic factors and two-nucleon amplitudes and further spectroscopic factors from shell model calculations with the modified GLEK interaction [12, 14, 25]. Even though this calculation does not reproduce the details of the structure of $^{96}$Sr, it gives us an estimation of the total strength to $0^+$ states ($\sigma(0_1^+) = 2.8$ mb). The calculated DWBA cross section for a pure $\Delta L = 0$ $(2s_{1/2})^2$ or $(1d_{3/2})^2$ of 0.85 and 0.64 mb, respectively, corresponding to several hundred counts expected. For the $^{96}$Sr$(t, p)$ reaction, based on the $6 \cdot 10^4$ pps intensity obtained in the past [9, 21], the measurement might also be feasible.

# 4 Required beam development

The ISOLDE yield database only provides one data point for $^{102}$Sr. Yields measured at the SC are several $10^8/\mu C$ for $^{94,95}$Sr with a UC$_x$ target. FLUKA simulation suggest that the in-target production is relatively constant in this mass region of Sr isotopes [26]. The measured yield

for $^{96}$Sr $5.7 \cdot 10^6/\mu C$ (again with SC) is affected by the much shorter half-life of this isotope, suggesting that the release is slow.

$^{96,98}$Sr beams have been previously used at Miniball [9, 21] and the intensity at the secondary target amounted to $7 \cdot 10^3$ and $6 \cdot 10^4$ pps for $^{96}$Sr and $^{98}$Sr, respectively. These two isotopes were produced by very different mechanisms. $^{96}$Sr was extracted as a SrF molecule from the target. The beam was separated using HRS tuned to mass 115 and the molecules were broken in the EBIS. The resulting accelerated $^{96}$Sr beam was pure. A different method was applied to $^{98}$Sr. Due to the short half-life and fast release of $^{98}$Rb, the $A = 98$ ions were cooled and stored in the REX-TRAP and then ionized in the EBIS. During the processing time most of the $^{98}$Rb decayed and the resulting beam contained 80% $^{98}$Sr [21].

At TRIUMF, the $^{94,95,96}$Sr beams were produced using TRILIS to selectively ionize the Sr compared to surface-ionized contamination. For $^{95}$Sr, a purity of 95% was achieved [14].

We propose to test the different possible production methods for neutron-rich Sr. Both methods, laser ionization and extraction as a molecule, should be compared and the contaminations for different mass numbers should be investigated. Such a study is required in order to decide on the best strategy for the planned measurements.

# 5    Beam time request

For the yield measurements using both methods we require:

- 2 shifts of stable beam tuning

- 1 shift to investigate the laser on/off effect

- 2 shifts for the molecular beam extraction

**Summary of requested shifts:**
We request 5 shifts (2 stable, 3 radioactive beam) for beam development.

# References

[1]  M. Wang, W. Huang, F. Kondev, G. Audi,  and S. Naimi, Chin. Phys. C **45**, 030003 (2021).

[2]  P. Campbell, H. L. Thayer, J. Billowes, P. Dendooven, *et al.*, Phys. Rev. Lett. **89**, 082501 (2002).

[3]  P. Garrett, E. Clement,  and M. Zielińska, Prog. Part. Nucl. Phys., submitted.

[4]  P. Federman and S. Pittel, Phys. Lett. B **69**, 385 (1977).

[5]  K. Heyde and J. L. Wood, Rev. Mod. Phys. **83**, 1467 (2011).

[6]  T. Togashi, Y. Tsunoda, T. Otsuka,  and N. Shimizu, Phys. Rev. Lett. **117**, 172502 (2016).

[7]  H. Mach, F. Wohn, G. Molnar, K. Sistemich, *et al.*, Nucl. Phys. A **523**, 197 (1991).

[8]  A. Chester, G. Ball, R. Caballero-Folch, D. S. Cross, *et al.*, Phys. Rev. C **96**, 011302(R) (2017).

[9] E. Clément, M. Zielińska, A. Görgen, W. Korten, *et al.*, Phys. Rev. Lett. **116**, 022701 (2016).

[10] J.-M. Régis, J. Jolie, N. Saed-Samii, N. Warr, *et al.*, Phys. Rev. C **95**, 054319 (2017).

[11] F. Buchinger, E. B. Ramsay, E. Arnold, W. Neu, *et al.*, Phys. Rev. C **41**, 2883 (1990).

[12] S. Cruz, P. Bender, R. Krücken, K. Wimmer, *et al.*, Phys. Lett. B **786**, 94 (2018).

[13] Y. Tsunoda, Private Communication (2021).

[14] S. Cruz, K. Wimmer, P. C. Bender, R. Krücken, *et al.*, Phys. Rev. C **100**, 054321 (2019).

[15] A. Esmaylzadeh, J.-M. Régis, Y. H. Kim, U. Köster, *et al.*, Phys. Rev. C **100**, 064309 (2019).

[16] G. Jung, "Nuclear Spectroscopy on Neutron Rich Rubidium With Even Mass Numbers," PhD thesis, Justus Liebig-Universitat, Giessen (1980).

[17] S. Cruz, K. Wimmer, S. S. Bhattacharjee, P. C. Bender, *et al.*, Phys. Rev. C **102**, 024335 (2020).

[18] J. Park, A. B. Garnsworthy, R. Krücken, C. Andreoiu, *et al.*, Phys. Rev. C **93**, 014315 (2016).

[19] H. Mach, M. Moszynński, R. Gill, F. Wohn, *et al.*, Phys. Lett. B **230**, 21 (1989).

[20] A. G. Smith, J. L. Durell, W. R. Phillips, M. A. Jones, *et al.*, Phys. Rev. Lett. **77**, 1711 (1996).

[21] E. Clément, M. Zielińska, S. Péru, H. Goutte, *et al.*, Phys. Rev. C **94**, 054326 (2016).

[22] E. M. F. Schussler, J.A. Pinston, A. Moussa, *et al.*, Nucl. Phys. A **339**, 415 (1980).

[23] K. L. Kratz, H. Ohm, A. Schröder, H. Gabelmann, *et al.*, Zeit. f. Phys. A **312**, 43 (1983).

[24] G. Lhersonneau, B. Pfeiffer, K.-L. Kratz, H. Ohm, *et al.*, Zeit. f. Phys. A **337**, 149 (1990).

[25] H. Mach, E. K. Warburton, R. L. Gill, R. F. Casten, *et al.*, Phys. Rev. C **41**, 226 (1990).

[26] J. Ballof, J. Ramos, A. Molander, K. Johnston, *et al.*, Nucl. Instr. Meth. B, in press, https://doi.org/10.1016/j.nimb.2019.05.044.

# Appendix

**DESCRIPTION OF THE PROPOSED EXPERIMENT**

The experimental setup comprises: (*name the fixed-ISOLDE installations, as well as flexible elements of the experiment*)

| Part of the | Availability | Design and manufacturing |
|---|---|---|
| (if relevant, name fixed ISOLDE installation: MINIBALL + only CD, MINIBALL + T-REX) | ☒ Existing | ☒ To be used without any modification |
| [Part 1 of experiment/ equipment] | ☐ Existing | ☐ To be used without any modification<br>☐ To be modified |
| | ☐ New | ☐ Standard equipment supplied by a manufacturer<br>☐ CERN/collaboration responsible for the design and/or manufacturing |
| [Part 2 of experiment/ equipment] | ☐ Existing | ☐ To be used without any modification<br>☐ To be modified |
| | ☐ New | ☐ Standard equipment supplied by a manufacturer<br>☐ CERN/collaboration responsible for the design and/or manufacturing |
| [insert lines if needed] | | |

HAZARDS GENERATED BY THE EXPERIMENT (if using fixed installation:) Hazards named in the document relevant for the fixed [MINIBALL + only CD, MINIBALL + T-REX] installation.

Additional hazards:

| Hazards | [Part 1 of experiment/ equipment] | [Part 2 of experiment/ equipment] | [Part 3 of experiment/ equipment] |
|---|---|---|---|
| **Thermodynamic and fluidic** | | | |
| Pressure | [pressure][Bar], [volume][l] | | |
| Vacuum | | | |
| Temperature | [temperature] [K] | | |
| Heat transfer | | | |
| Thermal properties of materials | | | |
| Cryogenic fluid | [fluid], [pressure][Bar], [volume][l] | | |
| **Electrical and electromagnetic** | | | |
| Electricity | [voltage] [V], [current][A] | | |
| Static electricity | | | |

| | | | |
|---|---|---|---|
| Magnetic field | [magnetic field] [T] | | |
| Batteries | ☐ | | |
| Capacitors | ☐ | | |
| **Ionizing radiation** | | | |
| Target material [material] | | | |
| Beam particle type (e, p, ions, etc) | | | |
| Beam intensity | | | |
| Beam energy | | | |
| Cooling liquids | [liquid] | | |
| Gases | [gas] | | |
| Calibration sources: | ☐ | | |
| • Open source | ☐ | | |
| • Sealed source | ☐ [ISO standard] | | |
| • Isotope | | | |
| • Activity | | | |
| Use of activated material: | | | |
| • Description | ☐ | | |
| • Dose rate on contact and in 10 cm distance | [dose][mSV] | | |
| • Isotope | | | |
| • Activity | | | |
| **Non-ionizing radiation** | | | |
| Laser | | | |
| UV light | | | |
| Microwaves (300MHz-30 GHz) | | | |
| Radiofrequency (1-300 MHz) | | | |
| **Chemical** | | | |
| Toxic | [chemical agent], [quantity] | | |
| Harmful | [chem. agent], [quant.] | | |
| CMR (carcinogens, mutagens and substances toxic to reproduction) | [chem. agent], [quant.] | | |
| Corrosive | [chem. agent], [quant.] | | |
| Irritant | [chem. agent], [quant.] | | |
| Flammable | [chem. agent], [quant.] | | |
| Oxidizing | [chem. agent], [quant.] | | |
| Explosiveness | [chem. agent], [quant.] | | |
| Asphyxiant | [chem. agent], [quant.] | | |

| | | | |
|---|---|---|---|
| Dangerous for the environment | [chem. agent], [quant.] | | |
| **Mechanical** | | | |
| Physical impact or mechanical energy (moving parts) | [location] | | |
| Mechanical properties (Sharp, rough, slippery) | [location] | | |
| Vibration | [location] | | |
| Vehicles and Means of Transport | [location] | | |
| **Noise** | | | |
| Frequency | [frequency],[Hz] | | |
| Intensity | | | |
| **Physical** | | | |
| Confined spaces | [location] | | |
| High workplaces | [location] | | |
| Access to high workplaces | [location] | | |
| Obstructions in passageways | [location] | | |
| Manual handling | [location] | | |
| Poor ergonomics | [location] | | |

Hazard identification:

Average electrical power requirements (excluding fixed ISOLDE-installation mentioned above): [make a rough estimate of the total power consumption of the additional equipment used in the experiment]: ... kW